Direct Low-Temperature Integration of Nanocrystalline Diamond with GaN Substrates for Improved Thermal Management of High-Power Electronics

Vivek Goyal, Anirudha V. Sumant, Desalegne Teweldebrhan, and Alexander A. Balandin**

A novel approach for the direct synthetic diamond–GaN integration via deposition of the high-quality nanocrystalline diamond films directly on GaN substrates at temperatures as low as 450–500 °C is reported. The low deposition temperature allows one to avoid degradation of the GaN quality, which is essential for electronic applications The specially tuned growth conditions resulted in the large crystalline diamond grain size of 100–200 nm without coarsening. Using the transient "hot disk" measurements it is demonstrated that the effective thermal conductivity of the resulting diamond/GaN composite wafers is higher than that of the original GaN substrates at elevated temperatures. The thermal crossover point is reached at ≈95–125 °C depending on the thickness of the deposited films. The developed deposition technique and obtained thermal characterization data can lead to a new method of thermal management of the high power GaN electronic and optoelectronic devices.

1. Introduction

Gallium nitride (GaN) attracts major attention for its wide range of the existing and potential electronic and optoelectronic applications. GaN, with a large bandgap of 3.4 eV, possesses a very high breakdown voltage (3×10^6 V cm^{-1}) and an extremely high peak (3×10^7 cm s^{-1}) and saturation velocity (1.5×10^7 cm s^{-1}).[1] These unique properties along with the high electron mobility observed in AlGaN/GaN heterostructures (2019 cm^2 V^{-1} s^{-1})[2] make GaN a superior material to Si and GaAs for the high-temperature high-power electronic devices, ultrahigh power switches, and microwave-power sources.[3] However, self-heating limits the performance of GaN devices and further development of GaN technology.[4,5] The temperature rise in high-power AlGaN/GaN heterostructure field-effect transistors (HFETs), which is currently on order of ≈180 °C,[6] continues to increase with growing current densities and shrinking device sizes.

For this reason, reliable performance of such devices depends on heat dissipation in the device active regions, which, in turn, depends on the thermal conductivity of GaN and common substrates used for its growth, e.g., silicon (Si), sapphire (Al_2O_3), or silicon carbide (SiC). Most recently, GaN-on-diamond wafers have been proposed as alternatives to conventional GaN/SiC offering improved thermal management.[7] Numerous approaches have been explored to integrate diamond with GaN including wafer-bonding, which involves either physical bonding GaN substrate with diamond wafers through some interlayer[8] or direct deposition of diamond films on GaN.[9] In the first case, the bonding process is critical, costly, and involves an additional dielectric adhesive layer of ≈50-nm thickness. This interlayer of a dissimilar material acts as a thermal barrier making it less efficient in the heat transfer In the second case, high substrate temperature required for the diamond deposition (≈800 °C) leads to GaN degradation owing to either diffusion of carbon (C) atoms to the GaN lattice or loss of nitrogen (N) from GaN resulting in the decreased GaN material quality. Moreover, it has been shown that lowering temperature below 600 °C using conventional H_2/CH_4 based growth chemistry results in the growth of the poor-quality diamond.[9] It is therefore crucially important to develop a method for the growth of the high-quality diamond films on GaN substrate at reasonably low substrate temperatures (400–500 °C).

In this work, we present a novel approach for the direct diamond–GaN integration based on nanocrystalline diamond (NCD) films growth using $Ar/CH_4/H_2$ gas chemistry. We succeeded in depositing high-quality NCD films directly on GaN substrates at low substrate temperatures of 450–500 °C. A special feature of NCD films was a relatively large diamond grain size of 100–200 nm, which is beneficial for thermal management. Conventional NCD films have smaller grain sizes of 10–100 nm.[10] We have experimentally shown that the effective thermal conductivity of the resulting NCD-on-GaN is better than that of the original GaN substrate at elevated temperatures. The thermal crossover point, where the effective thermal conductivity of NCD/GaN composite substrates outperforms that

Dr. V. Goyal,[+] Dr. D. Teweldebrhan,[++]Prof. A. A. Balandin
Nano-Device Laboratory
Department of Electrical Engineering and Materials Science and Engineering Program
University of California–Riverside, Riverside, CA 92521 USA
E-mail: balandin@ee.ucr.edu
Dr. A. V. Sumant
Center for Nanoscale Materials
Argonne National Laboratory, IL, 60439 USA
E-mail: sumant@anl.gov
[+] Present address: Texas Instruments, Dallas, TX 75243 USA
[++] Present address: Intel Corporation, Hillsboro, OR, USA

DOI: 10.1002/adfm.201102786

of GaN, is reached in the range $T \approx 95$–125 °C depending on the thickness of the deposited NCD films. This cross-over temperature is lower than the operating temperature ($T \approx 180$ °C) of GaN based HFETs, which clearly indicates the advantage offered by thin NCD films for efficient thermal management of GaN high-power high-temperature devices.

2. Sample Preparation and Characterization

We have grown NCD films of different thickness on free-standing single-crystal GaN substrates (480 μm thickness). The growth of NCD films were performed in a 915 MHz large-area microwave plasma chemical vapor deposition (MPCVD) system (DiamoTek 1800 series 915 MHz, 10 KW from Lambda Technologies Inc.) in the clean room environment. Prior to the growth, GaN substrates were deposited with a 10-nm thick tungsten layer using a sputter deposition process followed by the seeding treatment using the commercially available nano-diamond containing solution (source ITC, Raleigh, NC). This is a part of the process that we have developed for the growth of the low temperature nanocrystalline diamond film on a given substrate. More details about the MPCVD system and seeding process for low temperature growth are given elsewhere.[11]

The conventional NCD films are generally grown in the hydrogen (H) rich environment using H_2/CH_4 gas chemistry.[10] The growth conditions for our films were different. We used the argon-rich environment consisting of $Ar/CH_4/H_2$ gas chemistry. It is well-known that the addition of hydrogen gas above 5 vol% to the Ar/CH_4, mixture in an MPCVD process results in the systematic increase in the grain size of ultrananocrystalline diamond (UNCD) with an increase in the hydrogen concentration due to the suppression of re-nucleation rate leading to a transition of UNCD in to nanocrystalline and eventually to the microcrystalline diamond phase. However, this effect was previously observed at higher substrate temperatures of ≈800 °C.[12] In the present case, we have observed a similar trend in the grain size evolution even at low (T = 450 °C) substrate temperatures. More importantly, we were able to tune the diamond grain size to ≈150 nm using 4.5% hydrogen into the Ar/CH_4 gas mixture without the coarsening effect. This allowed us to deposit NCD films by varying NCD film thickness without any measurable change in the average grain size.

Based on our analysis of the growth conditions we concluded that the Ar-rich method of growing NCD at low temperature is more favorable for achieving NCD growth on GaN as opposed to H_2 rich method. We succeeded not only in reducing the total concentration of reactive atomic hydrogen in the growth chamber but also slowed down reaction kinetics due to the retarded surface diffusion process at low temperatures. Both of these facts are important for achieving the high-quality NCD growth on GaN without any adverse effects and for keeping the GaN structure unaffected in an aggressive environment of the diamond CVD process. In our Ar-based method the grain size of the diamond can be controlled from 2–5 nm to 2–3 μm by varying the Ar/H_2 ratio in the gas phase. However, at higher grain size (above 300 nm), the grain coarsening process starts to dominate, which means that the grain size cannot be kept constant with increasing film thickness. The initial characterization of the GaN substrate carried out using Raman spectroscopy before and after the growth of NCD film confirmed that the intrinsic structure of GaN was indeed well preserved and had not changed during the diamond growth process.

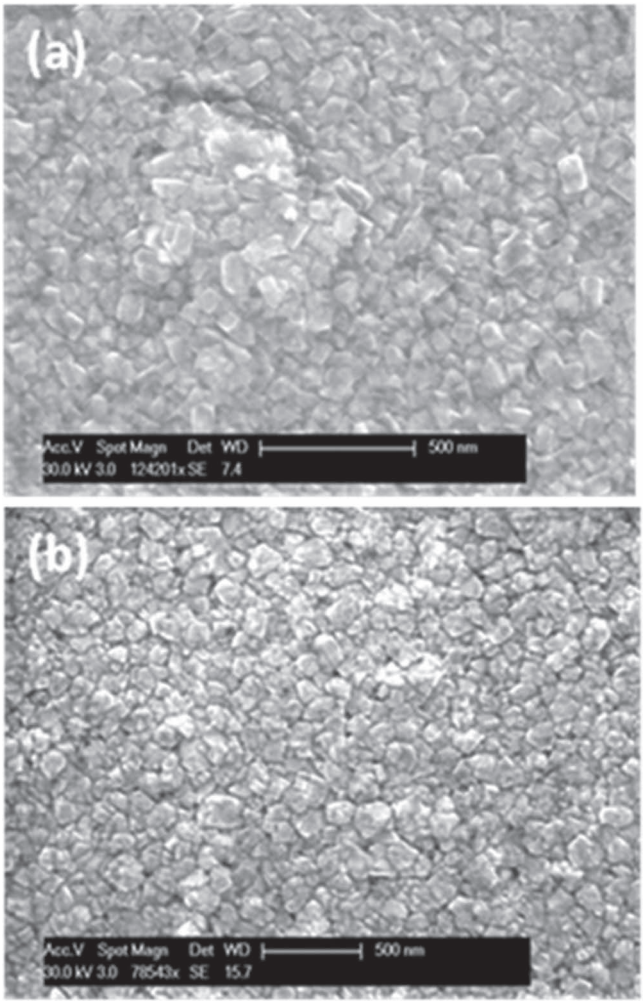

Figure 1. Top-view SEM images of two NCD films with different thicknesses: a) 150 nm and b) 300 nm. Note that in both samples the grain size is ≈150 nm.

The material characterization of NCD/GaN samples was performed using the high-resolution field-emission scanning electron microscope (XL-30 FEG) operated at 30 kV. **Figure 1** show the scanning electron microscopy (SEM) images of NCD films on GaN with two different thicknesses: a) 150 nm and b) 300 nm. The images reveal that the grain sizes for both NCD films with different thicknesses are on the order of ≈100 to 200 nm. The latter signifies no grain size change with the change in the thickness, which is not the case for microcrystalline diamond (MCD). The thickness of NCD films was verified using the cross-sectional focused ion beam (FIB) slicing and SEM imaging as shown in **Figure 2**. A thin layer of Pt was deposited locally on the NCD using FIB to obtain a much better edge resolution by avoiding the redeposition during the FIB cut.

Raman spectroscopy was performed to assess annealing induced damage that may have occurred in GaN during the

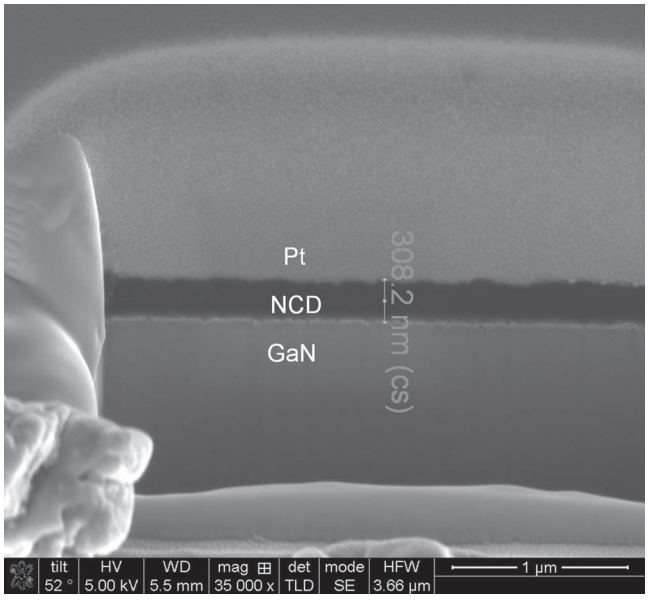

Figure 2. SEM image showing FIB cross-section of the NCD/GaN sample confirming the total thickness of NCD.

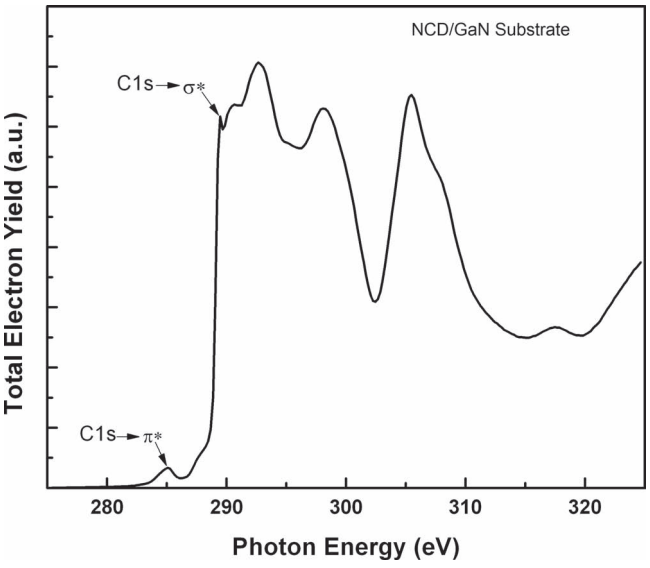

Figure 4. NEXAFS spectra taken on NCD film grown on GaN indicating the good quality diamond with the highly sp^3 bonding character. The spectrum was acquired in the total-electron yield mode.

diamond deposition. **Figure 3** shows the Raman spectra of a GaN wafer before deposition of NCD layer and after deposition. It is clear that the main GaN peaks such as E_2 (high) at 565 cm^{-1} and A_1(LO) at 737 cm^{-1} do not change. The spectrum after NCD deposition also shows the characteristic signatures of NCD deposited at lower substrate temperature. Previously, Raman spectroscopy has been used extensively for characterization of the diamond films and extraction of the sp^3/sp^2 ratio. However, in the case of nanocrystalline diamond, it is well-known that due to the smaller grain size and increased grain boundary volume, the visible Raman spectra is dominated by the sp^2 bonded carbon. It is explained by the larger Raman scattering cross-section for sp^2 bonded carbon than that for sp^3 carbon. For this reason it is difficult to determine the sp^3/sp^2 ratio in NCD quantitatively based on the Raman data alone. In such case, the near-edge X-ray absorption fine structure spectroscopy (NEXAFS), which utilizes the synchrotron X-rays can be used. **Figure 4** presents NEXAFS data for our samples indicating their quality. Unlike Raman spectroscopy, NEXAFS is equally sensitive to sp^3 and sp^2 bonded carbon as well as other bonding types. Since NEXAFS probes the local pertubed core-shell density of unoccupied states, the spectra obtained from the diamond and graphite are very different due to the distinct structures of their unoccupied electronic states. The NEXAFS spectra was taken in the total electron yield (TEY) mode with an incident photon beam normal to the substrate. Appropriate care was taken to correct for the signal resulting from carbon contamination in the beam-line optics. In Figure 4, the C1s NEXAFS spectra cleary shows the sharp diamond exciton at 289.3 eV due to the Cls→σ* transition and a pronounced dip at 302 eV due to the second band gap of diamond indicating the high-quality sp^3 bonded diamond and a small peak at 285 eV due to the C1s→π* transition indicating a presence of the small fraction of sp^2 bonded carbon at the grain boundaries. A small shoulder at 287.5 eV is due to the 1s→σ* resonance of the C-H bond suggesting that the surface is mostly H-terminated.[13,14] The calculation of sp^3 fraction from the NEXAFS spectra yielded a value of ≈99% confirming the high quality of NCD.

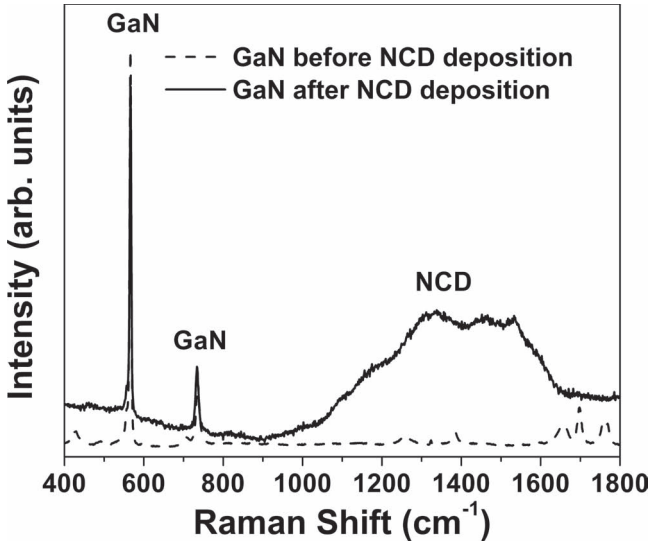

Figure 3. Raman spectra of GaN substrate before and after NCD deposition demonstrating no loss of GaN structure and quality after the diamond deposition. The data were recorded under 632.8-nm excitation in the backscattering configuration.

3. Thermal Measurements and Results

The thermal conductivity measurements of NDC/GaN substrates were carried out using two different experimental techniques: the transient plane source (TPS) technique (Hot

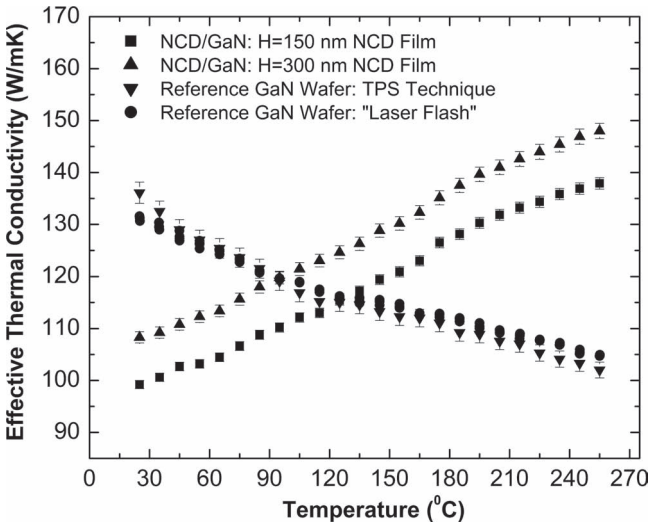

Figure 5. Effective thermal conductivity as a function of temperature for two NCD/GaN composite substrates and the reference GaN wafer. The error bars represent the data scattering based on ten measurements taken at each temperature.

Disk AB) and the "laser-flash" (Netzsch LFA). Both techniques have been calibrated with a home made 3-ω method,[15–17] which is considered to be a standard technique for measuring the thermal conductivity of thin films. We have previously successfully used the 3-ω setup for measuring the thermal conductivity of the ultra-nanocrystalline diamond (UNCD) films on Si.[15,18] The TPS measurements have been used for UNCD and MCD diamond films on Si.[19] The details of the experimental techniques and the measurement procedures are given in the Experimental Section.

Figure 5 presents the effective thermal conductivity $K_{eff}(T)$ as a function of temperature, T, for two NCD/GaN samples with NCD films of different thickness. The term "effective" is used to emphasize that the obtained value of the thermal conductivity is for the composite substrate consisting of GaN wafer and a layer of NCD. The K_{eff} value also includes the effect of the 10-nm thick tungsten layer between NCD and GaN and thermal boundary resistances (TBR) at all interfaces. The effective thermal conductivity value is related to the overall thermal resistance R_B of the composite substrate as $R_B = K_{eff}/H_T$, where H_T is the total thickness of the substrate.

For comparison, the thermal conductivity of the reference GaN wafer measured by both the TPS and "laser flash" techniques are also shown. One can see that the K values obtained for the GaN wafer are in agreement, which attests to the accuracy of our measurement procedures. The thermal conductivity of GaN wafer was found to be $K = 136$ W mK^{-1} at room temperature (RT). This value is in agreement with literature.[20] It is known that the thermal conductivity of GaN strongly depends on its crystal quality and concentration of defects and dislocations.[20] The monotonic decrease of K in GaN bulk with T is characteristic for semiconductor materials where thermal transport is limited by the crystal inharmonicity. In ideal crystals K is inversely proportional to temperature: $K \sim 1/T$. However in GaN, the $K(T)$ dependence is known to deviate from $1/T$ law owing to the acoustic phonon scattering on defects.[20]

On the other hand, the $K_{eff}(T)$ dependence for NCD/GaN is distinctively different. The effective thermal conductivity of the NCD/GaN composite substrates increases with temperature over the measured temperature range. This altered T dependence in polycrystalline materials such as NCD can be explained either by the conventional Callaway–Klemens approach, where the dominant mechanism restricting the thermal transport is the phonon scattering at the grains boundaries,[21,22] or by the phonon-hopping model proposed by Braginsky et al.,[23] which assumes that the phonon transport inside the grain follows the "bulk rules" while at the grain boundaries, the phonon transition rate from one grain to another through an inter-grain boundary increases with increasing T.[23] The TBR values also rapidly decrease with increasing temperature.

The difference in the thermal conductivity temperature dependence for the crystalline GaN and polycrystalline NCD results in the thermal crossover point, where the effective thermal conductivity of NCD/GaN composite substrate becomes larger than that of the reference GaN substrate. The thermal crossover point is reached at rather low $T \approx 125$ °C and further shifts to a lower $T \approx 95$ °C as the NCD thickness increases from 150 nm to 300 nm. This is an important observation, demonstrating that although composite NCD/GaN substrates are less thermally conductive than GaN at RT, they can become more efficient for heat spreading at the operating temperature of the state-of-the-art GaN based HFETs. A higher effective thermal conductivity of the composite substrate translates to the lower thermal resistance of the substrate, which is beneficial for heat removal from active GaN devices.

Another important observation is that the effective thermal conductivity of NCD/GaN substrates increases with increase in thickness of NCD films, which is in contrast to what was observed for UNCD/Si substrates.[19] The latter can be attributed to the higher thermal conductivity of NCD layer ($K \approx 500$–1400 W mK^{-1})[24,25] than that of GaN wafer itself ($K \approx 130$ W mK^{-1}).[26] This makes the effective thermal conductivity of the composite NCD/GaN wafers increase with increasing NCD thickness.The NCD films studied in this work have high thermal conductivity because of the large grain size of these samples ($D = 100$–200 nm). On the other hand, UNCD (with the grain size $D = 5$–10 nm) have very lower thermal conductivity, $K \approx 10$ W mK^{-1},[25,27] as compared to that of Si ($K \approx 150$ W mK^{-1})[19,28] resulting in the observed decrease in the effective thermal conductivity of UNCD/Si with an increase in UNCD thickness.[19]

In order to further analyze the physics behind the thickness dependence, we estimated the thermal conductivity in our NCD films using the Debye approximation, $K = (1/3)C_s v_g \partial$, where C_s is the specific heat capacity, v_g is the average phonon group velocity, and ∂ is the phonon mean free path (MFP) defined as $\partial = v_g \tau$, where τ is the phonon relaxation time.[29] The electronic contribution to the thermal conductivity of NCD films can be neglected because of their high electrical resistivity.[25] In NCD, the phonon MFP is limited by the grain size D. The simplest method for estimating K of NCD is to use the reported values of MFP and K in single-crystal diamond. Taking the MFP and K in diamond to be $\Lambda_D = 240$ nm and $K_D = 2000$ W mK^{-1}, respectively,[30] we can write $K_{NCD}/K_D = D/\Lambda_D \approx 100$ nm$/240$ nm $= 0.42$

This leads to $K_{NCD} \approx 0.42 \times 2000 = 833$ W mK^{-1} at RT. This is a rather high value due to the large grain size D in our samples. One can calculate K directly by taking the density and specific heat values to be 3.44 g cm^{-3}[[24]] and 0.511 J g^{-1} K^{-1}.[30] The group velocity can be assumed to be the same as the velocity of sound in NCD and taken to be 17980 m s^{-1}.[25] Alternatively, it can be estimated from the equation $\upsilon_g = (Y/\rho)^{1/2}$, where Y is the Young's modulus, which is ≈1120 GPa for NCD,[24] and ρ is the mass density, which gives $\upsilon_g \approx 18\,000$ m s^{-1}. Using these values, the lattice thermal conductivity of NCD with the large grain size is calculated to be $K \approx 1110$ W mK^{-1} at RT. Both estimates agree, within the uncertainty of the material characteristics, that the thermal conductivity of NCD with the grain size $D = 100$–200 nm is higher than that of GaN. The latter supports our experimental observations.

4. Conclusions

We demonstrated the low-temperature deposition of the high-quality nanocrystalline diamond films directly on GaN substrates. The low deposition temperature allows one to avoid degradation of the GaN quality. In order to improve the thermal properties of NCD films we tuned the growth conditions in such a way that the resulting films had the large grain size of 100–200 nm. The transient thermal measurements revealed that the composite GaN/NCD substrates are less thermally resistive at elevated temperatures than the reference GaN wafers. Our results suggest a new method for thermal management of the high-power GaN electronic and optoelectronic devices.

5. Experimental Section

The first experimental technique used for K measurements was the transient plane source technique ("hot disk"). During the measurements, a thin Ni heat-sensor encapsulated in a thin electrically insulating Kaptan film was sandwiched between two pieces of the sample under investigation. A short electric current was passed through the sensor to generate a heat wave, which propagated into the samples. The temperature rise in response to the dissipated heat was determined from the change in the resistance of the Ni sensor, which depended on the thermal properties of the surrounding sample. The temperature rise versus time was used to extract the thermal conductivity from the equation $\overline{\Delta T(\tau)} = P(\pi^{3/2} r K)^{-1} D(\tau)$, where τ is the parameter related to the thermal diffusivity α and the transient measurement time t_m through the expression $\tau = (t_m \alpha / r^2)^{1/2}$ and r is the radius of the sensor, P is the input power for heating the sample, and $D(\tau)$ is a modified Bessel function.[31]

The second laser-flash technique could give a value of the thermal conductivity, which was interpreted an average cross-plane component of the thermal conductivity tensor. During the experiment the sample was heated with short light pulses using an adjustable xenon flash lamp on one end. A contactless InSb IR detector measured the temperature rise on the other end of the sample. The thermal conductivity was estimated from expression $K = \alpha \rho C_p$, where α is the thermal diffusivity of the film determined in the experiment as $\alpha = 0.139 Z^2 / t_{1/2}$, $t_{1/2}$ is the measured half-rise time of temperature, C_p is the heat capacity, and ρ is the mass density of the material. For the numerical analysis of the experimental data several theoretical approaches were used including the Parker, Cowan, and Clark-Taylor analysis.[31] These analysis curves were plotted with the experimental temperature time rise in order to extrapolate diffusivity and correct the result for the heat loss to sidewalls of sample holder.

Acknowledgements

The work at UCR was supported by the US Office of Naval Research (ONR) through award No 00014-10-1-0224 on Heat Spreaders for GaN Power Electronics. Use of the Center for Nanoscale Materials was supported by the US Department of Energy (DOE) Office of Science and Office of Basic Energy Sciences under contract DE-AC02-06CH11357. A.V.S. thanks Il Woong from CNM for his help with the FIB cross-section measurements, Andy Konicek for taking NEXAFS spectra on the NCD/GaN samples, and Krishna Linga from Inphot Inc for providing single crystal GaN substrates. The NCD growth and characterization were performed in the Center for Nanoscale Materials at the Argonne National Laboratory (ANL). The NEXAFS spectra were taken at Brookheaven National Laboratory (BNL). The thermal measurements were conducted in the Nano-Device Laboratory at UCR.

Received: November 17, 2011
Published online: February 1, 2012

[1] B. Gelmont, K. Kim, M. Shur, *J. Appl. Phys.* **1993**, *74*, 1818.
[2] R. Gaska, J. W. Yang, A. Osinsky, Q. Chen, M. Asif Khan, A. O. Orlov, G. L. Snider, M. S. Shur, *Appl. Phys. Lett.* **1998**, *72*, 707.
[3] U. K. Mishra, L. Shen, T. E. Kazior, Y.-F. Wu, *Proc. IEEE* **1995**, *83*, 1306.
[4] a) K. Fillipov, A. A. Balandin, *MRS Internet J. Nitride Semicond. Res.* **2003**, *8*, 4; b) V. O. Turin, A. A. Balandin, *Electron Lett.* **2004**, *40*, 81; c) V. O. Turin, A. A. Balandin, *J. Appl. Phys.* **2006**, *100*, 054501.
[5] R. J. Trew, D. S. Green, J. B. Shealy, *IEEE Microwave Magn.* **2009**, *10*, 116.
[6] M. Kuball, J. M. Hayes, M. J. Uren, T. Martin, J. C. H. Birbeck, R. S. Balmer, B. T. Hughes, *IEEE Electron Device Lett.* **2002**, *23*, 7.
[7] J. G. Felbinger, M. V. S. Chandra, Y. Sun, L. F. Eastman, J. Wasserbauer, F. Faili, D. Babic, D. Francis, F. Ejeckam, *IEEE Electron Device Lett* **2007**, *28*, 948.
[8] a) D. Francis, F. Faili, D. Babi , F. Ejeckam, A. Nurmikko, H. D. Maris, *Diamond Relat. Mater.* **2010**, *19*, 229; b) D. Francis, J. Wasserbauer, F. Faili, D. Babi , F. Ejeckam, W. Hong, P. Specht, E. R. Weber, GaN HEMT epilayers on diamond substrates: Recent progress, *Proc. CS MANTECH Conf.*, Austin, TX, May 14-17,**2007**, pp. 133–136.
[9] P. W. May, H. Y. Tsai, W. N. Wang, J. A. Smith, *Diamond Relat. Mater.* **2006**, *15*, 526.
[10] J. E. Butler, A. V. Sumant, *Chem. Vap. Deposition* **2008**, *14*, 145.
[11] A. V. Sumant, O. Auciello, H.-C. Yuan, Z. Ma, R. W. Carpick, D. C. Mancini, *Proc. SPIE* **2009**, *7318*, 17.
[12] D. Zhou, D. M. Gruen, L. C. Qin, T. G. McCauley, A. R. Krauss, *J. Appl. Phys.* **1998**, *84*, 1981.
[13] A. V. Sumant, D. S. Grierson, J. E. Gerbi, J. Carlisle, O. Auciello, R. W. Carpick, *Phys. Rev. B* **2007**, *76*, 235429.
[14] X. Xiao, J. Birrell, J. E. Gerbi, O. Auciello, J. A. Carlisle, *J. Appl. Phys.* **2004**, *96*, 2232.
[15] M. Shamsa, S. Ghosh, I. Calizo, V. Ralchenko, A. Popovich, A. A. Balandin, *J. Appl. Phys.* **2008**, *103*, 083538.
[16] M. Shamsa, W. L. Liu, A. A. Balandin, C. Casiraghi, W. I. Milne, A. C. Ferrari, *Appl. Phys. Lett.* **2006**, *89*, 16192.
[17] S. Ghosh, D. Teweldebrhan, J. R. Morales, J. E. Garay, A. A. Balandin, *J. Appl. Phys.* **2009**, *106*, 113507.
[18] R. Ikkawi, N. Amos, A. Lavrenov, A. Krichevsky, D. Teweldebrhan, S. Ghosh, A. A. Balandin, D. Litvinov, S. Khizroev, *J. Nanoelectron. Optoelectron.* **2008**, *3*, 44.

[19] V. Goyal, S. Subrina, D. L. Nika, A. A. Balandin, *Appl. Phys. Lett.* **2010**, *97*, 031904.
[20] a) J. Zou, D. Kotchetkov, A. A. Balandin, D. I. Florescu, F. H. Pollak, *J. Appl. Phys.* **2002**, *92*, 2534; b) D. Kotchetkov, J. Zou, A. A. Balandin, D. I. Florescu, F. H. Pollak, *Appl. Phys. Lett.* **2001**, *79*, 4316.
[21] A. Khitun, A. A. Balandin, J. L. Liu, K. L. Wang, *J. Appl. Phys.* **2000**, *88*, 696.
[22] J. L. Liu, A. Khitun, K. L. Wang, W. L. Liu, G. Chen, Q. H. Xie, S. G. Thomas, *Phys. Rev. B* **2003**, *67*, 165333.
[23] L. Braginsky, N. Lukzen, V. Shklover, H. Hofmann, *Phys. Rev. B* **2002**, *66*, 134203.
[24] J. Philip, P. Hess, T. Feygelson, J. E. Butler, S. Chattopadhyay, K. H. Chen, L. C. Chen, *J. Appl. Phys.* **2003**, *93*, 2164.
[25] A. V. Sumant, O. Auciello, R. W. Carpick, S. Srinivasan, J. E. Butler, *MRS Bull.* **2010**, *35*, 281.
[26] E. K. Sichel, J. I. Pankove, *J. Phys. Chem. Solids* **1977**, *38*, 330.
[27] M. A. Angadi, T. Watanabe, A. Bodapati, X. Xiao, O. Auciello, J. A. Carlisle, J. A. Eastman, P. Keblinski, P. K. Schelling, S. R. Phillpot, *J. Appl. Phys.* **2006**, *99*, 114301.
[28] C. J. Glassbrenner, G. A. Slack, *Phys. Rev.* **1964**, *134*, A1058.
[29] P. G. Klemens, in *Solid State Physics*, Vol. 7, (Eds: F. Seitz, D. Turnbull), Academic, New York**1958**.
[30] V. Ralchenko, S. Pimonev, V. Konov, A. Khomich, A. Saveliev, A. Popovich, I. Vlasov, E. Zavedeev, A. Bozhko, E. Loubnin, R. Khmelnitskii, *Diamond Relat. Mater.* **2007**, *16*, 2067.
[31] S. E. Gustafsson, *Rev. Sci. Instrum.* **1991**, *62*, 797.